Biomedicine & Pharmacotherapy 140 (2021) 111747

Contents lists available at ScienceDirect

Biomedicine & Pharmacotherapy

journal homepage: www.elsevier.com/locate/biopha

Original article

Development of nitric oxide releasing visible light crosslinked gelatin methacrylate hydrogel for rapid closure of diabetic wounds

Alap Ali Zahid [a,b], Robin Augustine [a,b], Yogesh B. Dalvi [c], K. Reshma [c,d], Rashid Ahmed [a,b], Syed Raza ur Rehman [a,b], Hany E. Marei [e], Rashad Alfkey [f], Anwarul Hasan [a,b,*]

[a] Department of Mechanical and Industrial Engineering, College of Engineering, Qatar University, Doha 2713, Qatar
[b] Biomedical Research Center (BRC), Qatar University, Doha 2713, Qatar
[c] Pushpagiri Research Centre, Pushpagiri Institute of Medical Sciences & Research, Tiruvalla 689101, Kerala, India
[d] Department of Biotechnology St. Peter's College Kolenchery, Ernakulam 682311, Kerala, India
[e] Department of Cytology and Histology, Faculty of Veterinary Medicine, Mansoura University, Mansoura, Egypt
[f] Hamad Medical Corporation, Doha 3050, Qatar

ARTICLE INFO

Keywords:
GelMA
Nitric oxide
S-nitroso-N-acetylpenicillamine (SNAP)
Visible light photoinitiator
Diabetic wound healing

ABSTRACT

Management of non-healing and slow to heal diabetic wounds is a major concern in healthcare across the world. Numerous techniques have been investigated to solve the issue of delayed wound healing, though, mostly unable to promote complete healing of diabetic wounds due to the lack of proper cell proliferation, poor cell-cell communication, and higher chances of wound infections. These challenges can be minimized by using hydrogel based wound healing patches loaded with bioactive agents. Gelatin methacrylate (GelMA) has been proven to be a highly cell friendly, cell adhesive, and inexpensive biopolymer for various tissue engineering and wound healing applications. In this study, S-Nitroso-N-acetylpenicillamine (SNAP), a nitric oxide (NO) donor, was incorporated in a highly porous GelMA hydrogel patch to improve cell proliferation, facilitate rapid cell migration, and enhance diabetic wound healing. We adopted a visible light crosslinking method to fabricate this highly porous biodegradable but relatively stable patch. Developed patches were characterized for morphology, NO release, cell proliferation and migration, and diabetic wound healing in a rat model. The obtained results indicate that SNAP loaded visible light crosslinked GelMA hydrogel patches can be highly effective in promoting diabetic wound healing.

1. Introduction

Non-healing wounds are among serious complications of diabetes mellitus resulting in significant morbidity, mortality, and increased health care costs, caused by prolonged microbial infections and limb amputations [1]. According to the International Diabetes Federation (IDF) estimates reported in 2019, more than 463 million adults belonging to 20 and 79 age groups were suffering from diabetes mellitus, and the number is expected to cross 700 million by 2045 [2]. The delayed healing of diabetic wounds and ulcers occur due to multiple sets of factors, which includes but is not limited to decreased formation of the blood vessels [3] (lack of angiogenesis) [4], impaired secretion of growth factors, reduction in cell viability, slow cell migration, inadequate cell proliferation [5] and persistent microbial infections [6]. Numerous strategies such as protective wound dressings [7,8] or skin substitutes [9], application of growth factors, and the use of ointments containing antibiotics have been tried to overcome the above challenges and achieve faster healing of chronic diabetic wounds. However, many such approaches suffer from limitations which are evident from the continuous increase in diabetic chronic wound cases worldwide. Therefore, there is a dire need for advanced therapeutic modalities that could promote the healing of diabetic wounds.

It is essential to have plenty of pores in the wound healing patches to provide proper aeration, good swelling capacity to absorb excess exudates, keep the wound surface moist, and contain effective antibacterial agents for preventing infections [10]. A wide range of biodegradable synthetic polymers have been envisaged for wound dressing and wound healing patch development. However, many synthetic materials can cause localized cell death and significantly affect tissue regeneration [11,12]. Under these constraints, the development of bioactive and

* Corresponding author at: Department of Mechanical and Industrial Engineering, College of Engineering, Qatar University, Doha 2713, Qatar.
E-mail addresses: hasan.anwarul.mit@gmail.com, ahasan@qu.edu.qa (A. Hasan).

https://doi.org/10.1016/j.biopha.2021.111747

Available online 25 May 2021

cell-friendly biomaterial patches is of prime importance to provide an appropriate physiological environment that can support cell proliferation and tissue regeneration while protecting the wound from microbial infections [13–15].

Hydrogels possess huge potential for developing wound healing patches due to their 3D network structure, and supporting cell growth and tissue formation [16]. Hydrogels have been used in various biomedical applications, such as tissue engineering, regenerative medicine, drug delivery, and tissue adhesives [16,17]. Gelatin methacrylate (GelMA) is a promising hydrogel that can be used to develop wound healing patches [18,19]. GelMA is a methacrylated form of gelatin that undergoes radical induced photopolymerization and form crosslinked hydrogels [20]. Conventionally, various water-based photoinitiators such as 2-hydroxy-1-[4-(2-hydroxyethyl) phenyl]− 2-methyl-1--propanone (Irgacure 2959) and lithium acylphosphinate salt (LAP) that undergoes UV light irradiation have been used for GelMA crosslinking. However, reports have suggested that ultraviolet A (UVA) radiation (wavelength ranging from 320 to 400 nm) and ultraviolet B (UVB, wavelength ranging from 290 to 320 nm) may exert a damaging impact on cells [21–24]. Thus, to avoid UV light induced deleterious effects of photocrosslinking, researchers have recently devised a new range of visible light photocrosslinking methods to prepare cell-friendly scaffolds. For example, Lim et al. demonstrated a new visible-light photoinitiating system at the wavelength range of 400–450 nm [25]. They introduced ruthenium (Ru) based transition metal complex and sodium persulfate (SPS)-based salt for the photocrosslinking, where they reported high cell viability with visible light irradiation in comparison with UV crosslinked cell-laden constructs [25]. In the present study, we used Ru and SPS based photocrosslinking method for the fabrication of GelMA patches.

Nitric Oxide (NO) is one of the most important factors involved in biological systems such as cell proliferation, angiogenesis, and anti-inflammatory responses [26]. NO also possesses strong antibacterial potential, enabling this compound to be used for wound healing applications [26,27]. NO donor S-nitroso-N-acetylpenicillamine (SNAP) has been incorporated in wound healing patches to utilize the favourable effects of NO. It releases NO over long durations (> 3 weeks) and decreases thrombus formation at localized treatment sites when it is loaded within biomedical polymers [28]. Thus, when loaded in hydrogel patches, this potential of NO produced from its donors can be used to promote rapid wound healing.

In this work, a GelMA hydrogel based patch loaded with SNAP was developed to achieve rapid wound healing. The NO was released from the GelMA/SNAP hydrogel supported mammalian cell proliferation and migration and enhance wound healing in diabetic rat model. The release of NO from GelMA hydrogel and the ability to support cell proliferation and diabetic wound healing provide great potential for wound healing applications.

2. Experimental section

2.1. Materials

Gelatin (bovine skin origin, type B), methacrylic anhydride (MA), MTT dye, and live-dead cell staining kit were supplied from Sigma Aldrich (USA). Dialysis tubing of (14,000 Da molecular weight cut off) and dimethyl sulfoxide (DMSO) were purchased from fisher scientific (USA). S-nitroso-N-acetylpenicillamine (SNAP) of the biological grade was obtained from Tocris (USA). Ruthenium visible light photoinitiator of catalogue number 5248 (400–450 nm) was purchased from Advanced BioMatrix (USA). Dulbecco's Modified Eagle's Medium (DMEM) high glucose, fetal bovine serum (FBS), phosphate buffered saline (PBS), penicillin-streptomycin (10,000 U/mL), and trypsin-EDTA (0.25%, phenol red) were purchased from Gibco (USA).

2.2. Preparation of gelatin methacrylate polymer or GelMA

Gelatin derived from bovine skin was dissolved in PBS solution at 60°C with a concentration of 10% (w/v) [29,30]. Under stirred conditions at 50°C, 8 mL of MA was added for each 100 mL (8% v/v) of gelatin solution at 0.5 mL/min dropwise. The prepolymer solution was then reacted for 3 h. Dilution was performed to stop the reaction at 5X by adding 400 mL of PBS preheated at 50 °C. After that, salts and methacrylic acid were removed by allowing the mixture to be dialyzed against ultrapure deionized water for one week at 40 °C. The dialyzed solution was freeze dried for one week, resulting in a porous white foam of GelMA polymer kept at −80 °C until further use [30–32].

2.3. Preparation of SNAP loaded GelMA hydrogel

Freeze-dried GelMA was dissolved in PBS solution (1X) at a concentration of 2.5% and vortexed thoroughly to make a pre-hydrogel solution. SNAP with an optimized concentration of 10 μg/mL, 20 μg/mL, and 40 μg/mL were added to the pre-hydrogel solution and categorized as 0.5 G (GelMA-SNAP-0.04%, w/w), 1 G (GelMA-SNAP-0.08%, w/w) and 2 G (GelMA-SNAP-0.16%, w/w) respectively. Finally, the pre-hydrogel blends of SNAP and GelMA were crosslinked by using Ru and SPS based visible light crosslinking kit. Ru with a concentration of 20 mM with a volume of 20 μL was added and mixed to the pre hydrogel solution of 1 mL. In our observation, SPS in higher quantity was toxic to the cells; therefore, we optimized and used the minimal concentration of 50 mM SPS at 20 μL volume to the above pre hydrogel solution and vortex thoroughly. 50 μL of the obtained pre-hydrogel mixture was placed on a round glass slide and then exposed to normal torchlight (410– 440 nm) for 60 s to photocrosslink the free radicals of GelMA prepolymer chains.

2.4. Characterization of SNAP loaded GelMA hydrogel

2.4.1. Scanning electron microscopy (SEM)

The morphology of the developed hydrogel samples was assessed with the help of Scanning Electron Microscopy (SEM) named FEI Nova-NanoSEM. The hydrogel samples were fixed on the stubs using double-sided adhesive tape. Then, the sputter coating was carried out with up to 200–300 Å thickness of the gold layer to make the samples conductive. Later, the SEM was performed at an accelerating voltage of 20 kV.

2.4.2. Fourier transform infrared spectroscopy (FTIR)

Fourier transform infrared spectroscopy was used as a standard technique to evaluate the incorporation of various concentrations of NO inside the developed GelMA hydrogel samples. The samples were weighed up to 20 mg and used to determine the composition of samples such as blank GelMA, 0.5 G, 1 G, and 2 G SNAP containing hydrogel samples. The absorbance was recorded within a frequency range of 400–4000 cm^{-1} using an FTIR instrument labelled as PerkinElmer (USA). Extreme care was taken while recording the FTIR spectra within a resolution of ± 4 cm^{-1} while the scanning frequency was maintained 32 times at a room temperature [33].

2.4.3. X-Ray diffraction (XRD)

The X-ray diffraction (XRD) technique was used to ascertain the crystalline or amorphous nature of hydrogel samples such as blank GelMA, 0.5 G, 1 G, and 2 G NO loaded hydrogels with an Empyrean XRD system from Malvern Panalytical. The hydrogel samples of an approximate weight of 20 mg were placed in the holder. XRD spectrum of hydrogel samples was measured with a scanning rate between 5° and 118° adjusting a 0.032° step size while scanning range 2θ was fixed within a range of 0–60° using a 40 kV voltage and 30 mA current.

2.4.4. Determination of swelling properties of the patches

The swelling behaviour of hydrogel samples, including blank GelMA,

0.5 G, 1 G, and 2 G NO loaded GelMA hydrogels, were calculated using the gravimetric technique. The samples were adequately dried, followed by weighing, and placed in a distilled water inside the Petri dishes at room temperature. Later, the samples were taken out, appropriately dried with filter paper, and their weights were measured accordingly. The swelling potentials of the hydrogel samples were recorded as already described in our earlier publication [34]. The experiment was conducted for 50 h. All the samples were taken into triplicates for means and standard deviations.

2.4.5. Release study of NO loaded GelMA hydrogel

The release of NO from GelMA hydrogels was evaluated by Griess assay [13]. Dulbecco's phosphate-buffered saline (DPBS) was used to immerse the hydrogel samples, including blank GelMA hydrogel, 0.5 G, 1 G, and 2 G NO loaded GelMA hydrogel at 37 ºC, and pH 7.4. The samples analyte was later transferred into 96- well plate by adding 30 μL Griess reagent in each well of the 96-well plate. The incubation of samples was carried out for 30 min after treatment with Griess reagent. The reaction with the Griess reagent takes place following by changing the colour of the analyte to pink. The absorbance was recorded at 540 nm by using Epoch 2, a microplate spectrophotometer instrument. Later, a calibration curve was used to determine the release of NO after converting the recorded absorbance into nitrite concentrations.

2.5. In vitro cell proliferation and viability assays

Cell viability and proliferation rate were determined by live-dead and MTT assay with the samples of NO-releasing GelMA hydrogels. The experiments were performed with 3T3 fibroblasts and HaCaT keratinocyte cells for 1, 3, and 7 days. Initially, the cells with a density of 50×10^3 cells/mL were suspended into the 50 mL falcon tube. The sterile samples of blank GelMA, 0.5 G, 1 G, and 2 G hydrogels of size 10×10 mm were cut and placed into the 24 well cell culture treated plates. After that, the prepared suspensions were seeded on the hydrogels and incubated at 37 °C with 5% humidified CO_2. The experiments were performed in triplicates for statistical significance.

2.5.1. Live-dead cell staining assay

Cell viability and biocompatibility were determined using a Live-dead cell staining assay as per the manufacturer's (Invitrogen) reported protocol used in our earlier work [18]. In brief, 3T3 fibroblasts and HaCaT keratinocytes cells have been used for the study. In the first step, the dye was prepared by combining component A and component B. Then, 100 μL of dye was added to the 24 well plate of cell-seeded NO-releasing GelMA hydrogels. The plates were covered with aluminium foil and incubated for 30 min. Finally, the images of live and dead cells were captured using a fluoresce microscope (Olympus, FV300) at different resolutions.

2.5.2. MTT assay

At 1, 3, and 7 days of incubation intervals, the plates were taken out from the incubator, and the media were changed from the 24 well plates with the fresh media (450 μL). The prepared MTT dye (50 μL) was added to the respective well plates. The plates were covered with the aluminium foil and then incubated for 4 h at 37ºC. Then, the formazan crystals were dissolved in DMSO, and absorbance was recorded at 540 nm using a microplate reader. Then it was converted into cell proliferation rate by using Eq. (1) [13].

$$\text{Cell proliferation rate}\ (\%) = (OD\ of\ Sample / OD\ of\ Control) \times 100 \quad (1)$$

2.6. Cell migration by scratch assay

Cell migration assay was used for investigating the wound closure rate of scratch wounds generated on culture plates of 3T3 fibroblasts and HaCaT keratinocytes. A straight scratch was made with a 200 μL pipette tip when the cells were reached 90–95% confluency. The floating cells were aspirated and washed with DPBS, followed by the addition of fresh media. Next, GelMA hydrogel and NO loaded GelMA hydrogels weight samples around 20 mg were added to the well plates and incubated for 24 h at 37 °C with 5% CO_2. The images were captured using an Olympus X53 light microscope. The wound scratch gap was then determined using the Image J software, and the percentage of wound healing was calculated using Eq. (2).

$$\text{Wound Contraction}(\%) = \left(Wd^0 - Wd^t\right) / Wd^0 \times 100 \quad (2)$$

Where, $Wd^0 and Wd^t$ denotes the time interval of the wound scratch edges before and after time "t". The experiments were performed thrice for the statistical analysis (ANOVA).

2.7. In vivo study

2.7.1. Animal procurement and maintenance

We used 18 Sprague Dawley rats 8–10 weeks old for wound healing study in an animal model, having bodyweight around 190–230 g. These rats were procured from Kerala Veterinary College, Mannuthy, India, kept under uniform husbandry conditions of temperature (25 ± 5ºC), humidity ranging between 50% and 60%, and regular photoperiod (12:12 h dark: light cycle). Commercial pellet diet (Krish Scientist's Shoppe, Bangalore) and UV sterilized double filter water were provided *ad libitum*. Ethical approval was taken before conducting the experiments from Institutional Animal Ethics Committee (IAEC) and adhered strictly to the guidelines of the Committee for the Purpose of Control and Supervision of Experiments on Animal (No.602/PO/Re/S/2002/CPCSEA) as constituted by the Animal Welfare Division of Government of India. The animals were acclimatized for a period of 2 weeks with the environment.

2.7.2. Induction of diabetes

The 15 h fasting rats were made diabetic by intraperitoneal (IM) administration of nicotinamide (230 mg/ kg; Himedia) followed by streptozotocin (35 mg kg^{-1}; body weight; Sigma-Aldrich) [35]. After 48 h, blood glucose was estimated using a GOD-POD kit (Agappe Diagnostics, India). Rats with fasting blood glucose levels more than 150 mg/dl were considered diabetic and hence, used for the experiment [36]. The confirmed diabetic rats were divided randomly for the wound healing study.

2.7.3. Wound healing study on diabetic rats

General anesthesia with a combination of ketamine hydrochloride (50 mg kg^{-1}) and xylazine (5 mg kg^{-1}) was intraperitoneally given before surgical procedures. Before creating wounds, the dorsal surface of the animals was shaved using a sterile blade while the animals were under anesthesia. Povidone-iodine was used to disinfect the dorsal area. Four full-thickness punches were made in the skin using sterile surgical biopsy punches (10 mm) on the center of the dorsal shaved surface. One of the four wounds in each animal was treated with either GelMA-NO patches, blank GelMA patches, betadine (positive control), and normal saline (negative control), then covered with plain surgical tapes. Based on *in vitro* studies, 1 G (GelMA-SNAP-0.08%) NO loaded GelMA sample showed higher cell proliferation and migration and we selected this sample for the *in vivo* experiments. The wound size was measured every day and the animals were monitored thoroughly until the 21-day experimental period. The percentage of wound contraction was calculated as reported elsewhere in the literature [3,37].

On day 21st, the healed skin tissue samples were surgically collected for histopathological analysis using hematoxylin and eosin (H&E) staining. Finally, the images were captured with an Olympus light microscope.

3. Results and discussions

In this study, the rationale was to develop a NO-releasing visible light crosslinked GelMA based hydrogel to enhance diabetic and chronic wound healing. SNAP was used as a donor for releasing NO from the GelMA hydrogel. The successfully developed NO-releasing visible light crosslinked GelMA hydrogel for rapid closure of diabetic and chronic wounds is discussed below.

3.1. Morphology of hydrogel

The SEM images of blank GelMA, 0.5 G, 1 G, and 2 G lyophilized hydrogel samples crosslinked with Ru and SPS based visible light crosslinker were shown in Fig. 1a (i–iv). The sample's morphology shows a highly porous and honeycomb structure that is desirable for good wound healing properties. With the addition of SNAP, there was no significant difference found between the pores of the hydrogels [38].

3.2. FTIR analysis

The samples of blank GelMA, 0.5 G, 1 G, and 2 G hydrogels were further characterized using FTIR in attenuated total reflectance (ATR) mode was performed for determining the surface chemistry of developed hydrogels. Fig. 1-b displays the prominent amide bands of gelatin starting from N-H stretching vibration around 3292 cm−1 for the amide A, C-H stretching vibration around 3068 cm−1 for amide B, C=O stretching vibration around 1635 cm−1 for amide I, N-H deformation band around 1534 cm−1 for amide II and N-H deformation band around 1233 cm−1 for amide III [39]. The reaction of thiolactone of carboxyl group takes place with the primary amine group of gelatin forming a free thiol group which leads to producing the corresponding S-nitrosothiol [40]. This results in the attachment of SNAP with gelatin. On comparison of blank GelMA with NO-releasing hydrogels such as 0.5 G, 1 G, and 2 G exhibited a minor peak at around 1362 cm^{-1}. This explains the impregnation of SNAP into the GelMA hydrogel, which decreased the intermolecular association of the hydrogel network [13]. Taken together, the obtained absorption peaks have the same peaks as reported in an earlier study [13,41]. Thus, the FTIR peaks of the blank and NO-releasing hydrogels confirmed the coexistence of all the functional groups of gelatin, methacryloyl, and SNAP in the hydrogel.

3.3. XRD analysis

The crystalline and amorphous nature of the developed hydrogels were investigated by XRD. The characteristic peaks of blank GelMA, 0.5 G, 1 G, and 2 G NO-releasing hydrogels are given in Fig. 1-c. The blank sample of GelMA hydrogel did not show any sharp peak. Although it holds a minor peak at $2\theta = 32°$ links to the polymer structure as reported in our earlier study [13,20]. None of the samples have shown any sharp peaks indicating the amorphous structure of developed GelMA hydrogel patches. A further reduction in the intensity of broad diffraction patterns of GelMA was observed upon NO donor loading. This can be attributed to the further loosening of polymer chains by incorporated NO donor [42].

3.4. Swelling behaviour of GelMA hydrogel

The swelling behaviour of hydrogel holds a great value in several applications. It affects solute diffusion, surface, and mechanical properties as well as surface mobility [43]. On the other hand, the degree of

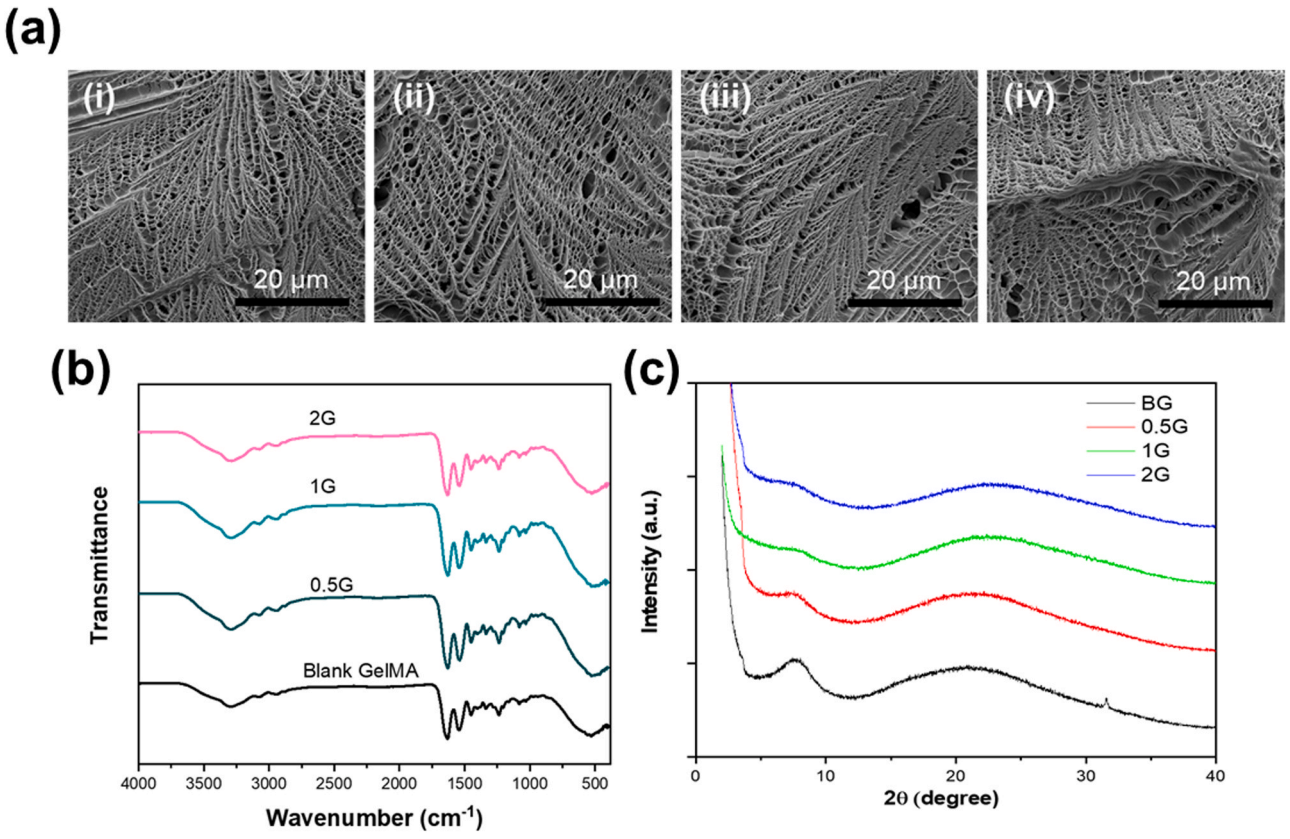

Fig. 1. Physical characterizations of the blank GelMA hydrogel, 0.5 G, 1 G, and 2 G NO releasing GelMA hydrogels. (a) SEM shows the porous honeycomb structure of (i) blank GelMA hydrogel, (ii) 0.5 G, (iii) 1 G, and (iv) 2 G. (b) FTIR spectra of the visible light crosslinked pure GelMA, 0.5 G, 1 G, and 2 G hydrogels, and (c) shows the XRD patterns of the hydrogel samples which shows the amorphous nature of the developed hydrogels. Samples 0.5 G, 1 G, and 2 G indicate GelMA hydrogels loaded with GelMA-SNAP-0.04%, GelMA-SNAP-0.08%, and GelMA-SNAP-0.16% of NO donor, respectively.

swelling highly depends on the pore size of the hydrogel network and the interaction between the polymers. For wound healing applications, the developed hydrogel must have high swelling behavior to help remove the wound exudates and reduce the chances of getting an infection. Fig. 2-a illustrates the swelling behavior of blank GelMA, 0.5 G, 1 G, and 2 G hydrogels. The graph was plotted using swelling ratio in percentage to time in hours. The experiment was carried out for 50 h as it is well understood that the GelMA is a highly hydrophilic biocompatible biopolymer [20]. The developed GelMA hydrogels in this study have also shown large swelling capacity, as evident from Fig. 2-a. Over time the swelling of the hydrogels increased gradually, with no significant change seen with the incorporation of NO in the hydrogel network.

3.5. Release of NO from the GelMA hydrogel

The Griess assay was used for determining the NO from the visible light crosslinked GelMA hydrogel. Fig. 2-b shows the NO release study from the blank GelMA, 0.5 G, 1 G, and 2 G NO impregnated GelMA hydrogels for up to 80 h at 37°C. As it is evident from the figure, NO was releasing gradually from the GelMA hydrogel. The release rate was higher where the SNAP concentrations were increased. For instance, going from ascending order 0.5 G, 1 G, and 2 G, the release was prolonged and continued. However, in the blank GelMA samples, there were no traces of NO. The initial fast release from the NO-GelMA samples was because of the existence of a SNAP donor on the surface of GelMA hydrogel that resulted in the rapid release. At 80 h of study, the release was reached 60%, 55%, and 45% for the 2 G, 1 G, and 0.5 G GelMA samples, respectively.

3.6. Increased cell proliferation and viability

3T3 fibroblasts and HaCaT keratinocytes have been used for cell viability and cell proliferation studies with our developed NO releasing visible light crosslinked GelMA hydrogels by using live-dead staining and MTT assay. Both cell types seeded on the developed hydrogels showed good viability and cell proliferation compared to the control samples. It was noticed that the 1 G and 2 G hydrogels showed enhanced cell viability in comparison with 0.5 G and blank GelMA hydrogels, as depicted in Fig. 3(a–b). The viable live cells were shown as green; however, the red dots indicate the dead cells. When reaching Day 7, the number of dead cells was higher in control and blank GelMA samples in both cell types. However, the NO releasing hydrogels reduced cell death and enhanced cell viability.

On the other hand, all the samples loaded with NO donor SNAP showed a higher number of cell proliferation and a relatively minor number of dead cells than control and blank GelMA samples. MTT assay results are shown in Fig. 3c (i–ii) for 3T3 and HaCaT cells. The assay was carried out for 1, 3, and 7 days. The fibroblast cells' results in Fig. 3c(i) showed improved cell proliferation for 1 G samples of GelMA hydrogels, which increased up to 140% until day seven compared to control, blank, 0.5 G, and 2 G GelMA hydrogels. The cell proliferation for HaCaT cells shown in Fig. 3c(ii) was initially decreased for the samples loaded with NO donor; however, the proliferation started increasing after day 3 for 1 G and 2 G GelMA hydrogels compared to control and blank GelMA samples.

Under normal physiological conditions, NO modulates the proliferation and recruitment of endothelial cells during angiogenic activity inside the body and thus helps in angiogenic activity [44]. The positive effect of NO occurs *via* various pathways and mechanisms, enhancing the encouragement of fibroblasts and keratinocytes movement through growth factors upregulation [45,46]. In this study, the growth of fibroblasts and keratinocytes was increased because of the exogenous release of NO from the GelMA hydrogel, which is triggered due to the iNOS pathway and epidermal growth factor [47]. However, detailed studies involving gene expression analysis are necessary to know the detailed mechanism behind this observation.

3.7. In vitro cell migration assay

In vitro scratch assay was used for studying the cell migration behaviour of 3T3 fibroblasts and HaCaT keratinocytes with the NO releasing GelMA hydrogels. The results are shown in Fig. 4. The qualitative results were depicted in Fig. 4a, and the quantified results were reported in Fig. 4b. The migration assay was performed for 24 h. In the case of fibroblasts, the wound scratch applied with 0.5 G, 1 G, and 2 G samples of NO releasing hydrogel have shown 54%, 78%, and 60% of wound contraction as compared to control and blank GelMA samples as evident in Fig. 4b(i). However, in HaCaT cells that followed the same wound contraction pattern as the fibroblast cells, 1 G and 2 G NO releasing GelMA hydrogel covered 50% and 34% of the wounds, respectively, compared to control samples. 0.08% (w/w) concentration of NO incorporated GelMA sample that is 1 G hydrogel showed considerably rapid closure of the scratch wound in fibroblast and

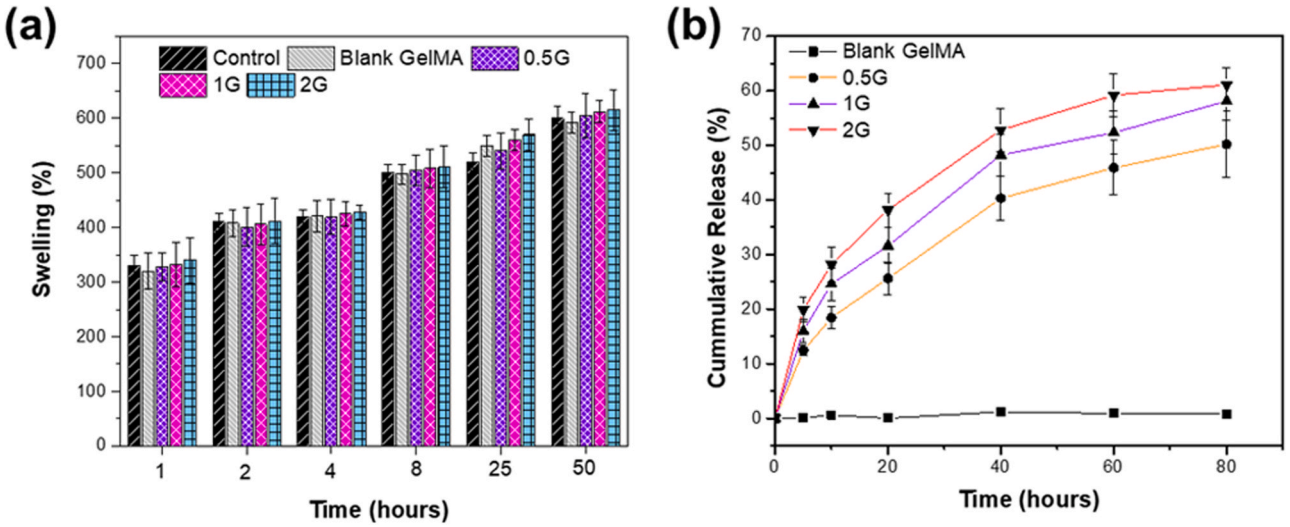

Fig. 2. (a) Shows the swelling studies of NO loaded visible light crosslinked GelMA based hydrogels, (b) displays the overall NO Release study throughout the period of 80 h at 37°C from blank GelMA hydrogel, 0.5 G, 1 G, and 2 G NO releasing GelMA based hydrogels. The SNAP impregnated GelMA hydrogels show prolonged and sustained NO release.

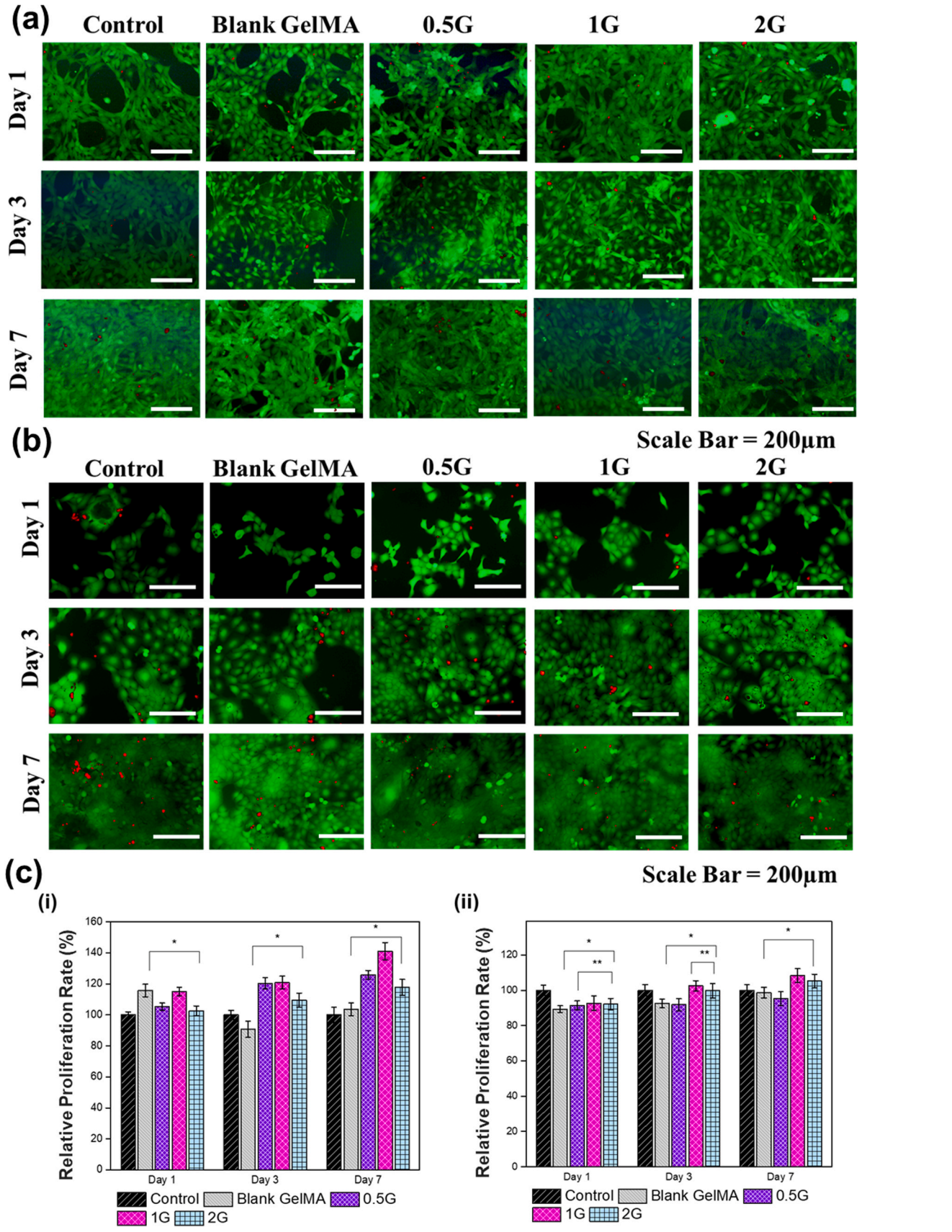

Fig. 3. Shows the increased cell viability of 3T3 fibroblasts (a) and HaCaT keratinocytes (b) using live/death cell staining assay. Fig (c) shows the relative cell proliferation rate in percentage, (i) shows the 3T3 fibroblast cells while (ii) displays the cell proliferation rate with HaCaT cells. The pictures were captured at 1, 3, and 7 days of incubation. All the experiments were performed in triplicates with p-value at * $P < 0.05$ and * * $P < 0.005$.

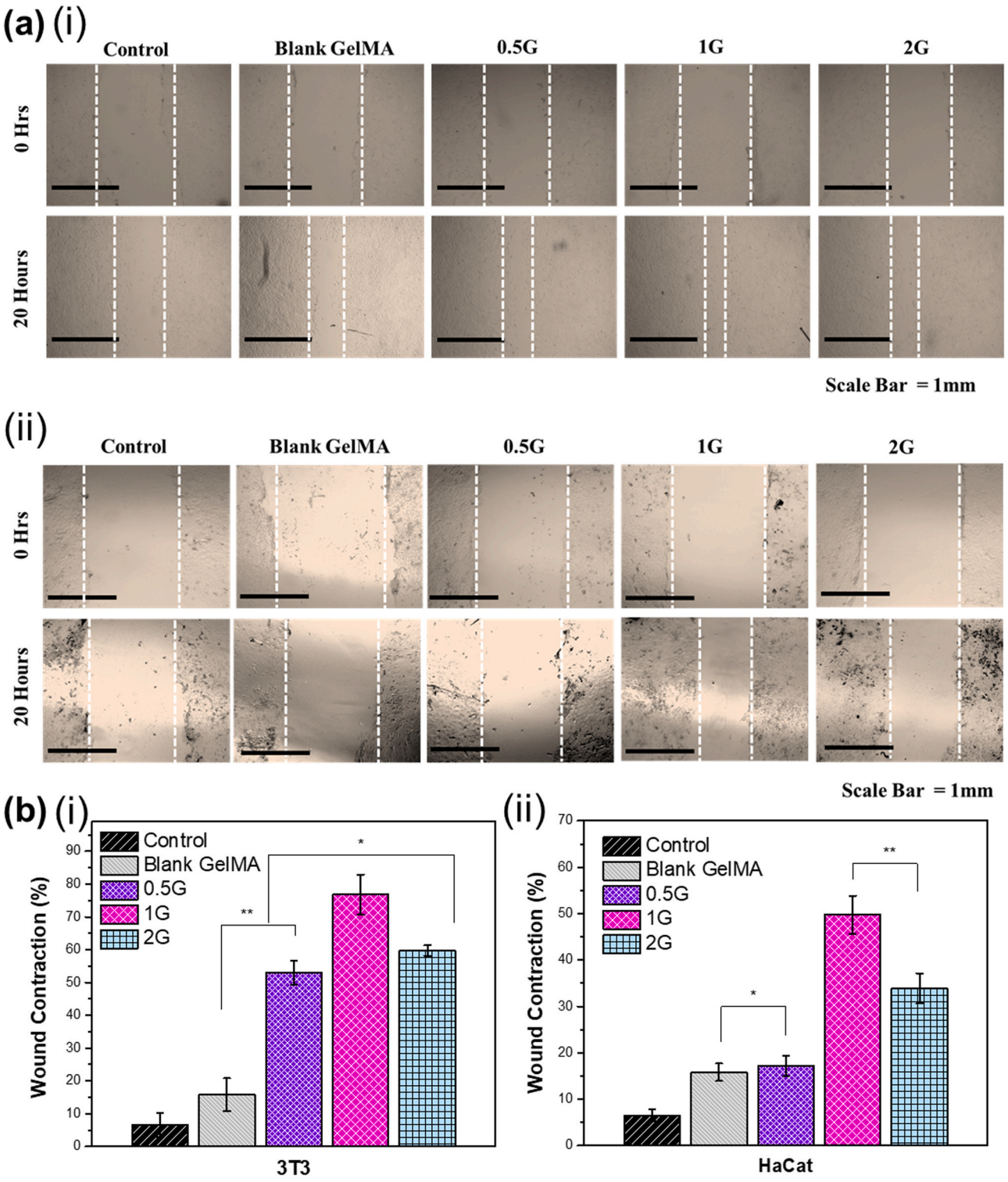

Fig. 4. Representation of cell migration performed by the scratch assay. (a) Images show the scratch on the (i) 3T3 fibroblast cells and (ii) HaCaT keratinocyte cells. (b) shows the quantified results of the cell migration images by using the Image J software (i) fibroblasts and (ii) keratinocytes. All the experiments were performed in triplicates with p-value at *P < 0.05 and ** P < 0.005.

keratinocyte cells as shown in Fig. 4b (i–ii). On the other hand, blank GelMA and 0.5 G GelMA could not heal the scratched area in keratinocytes cells as compared to 1 G samples. The optimum quantity of NO in GelMA hydrogel has resulted in faster cell proliferation and migration which are good indicators for the accelerated re-epithelialization process.

3.8. Outcome of in vivo wound healing experiment

In vivo wound healing experiment was performed on diabetes-induced Sprague Dawley rats, and the results are given in Fig. 5. The wound site of the diabetic rats looked bruising, slight bleeding, and epithelial damage caused by the incision on the first day of study (Fig. 5A). However, on the 7th day, all the wounds showed a sign of

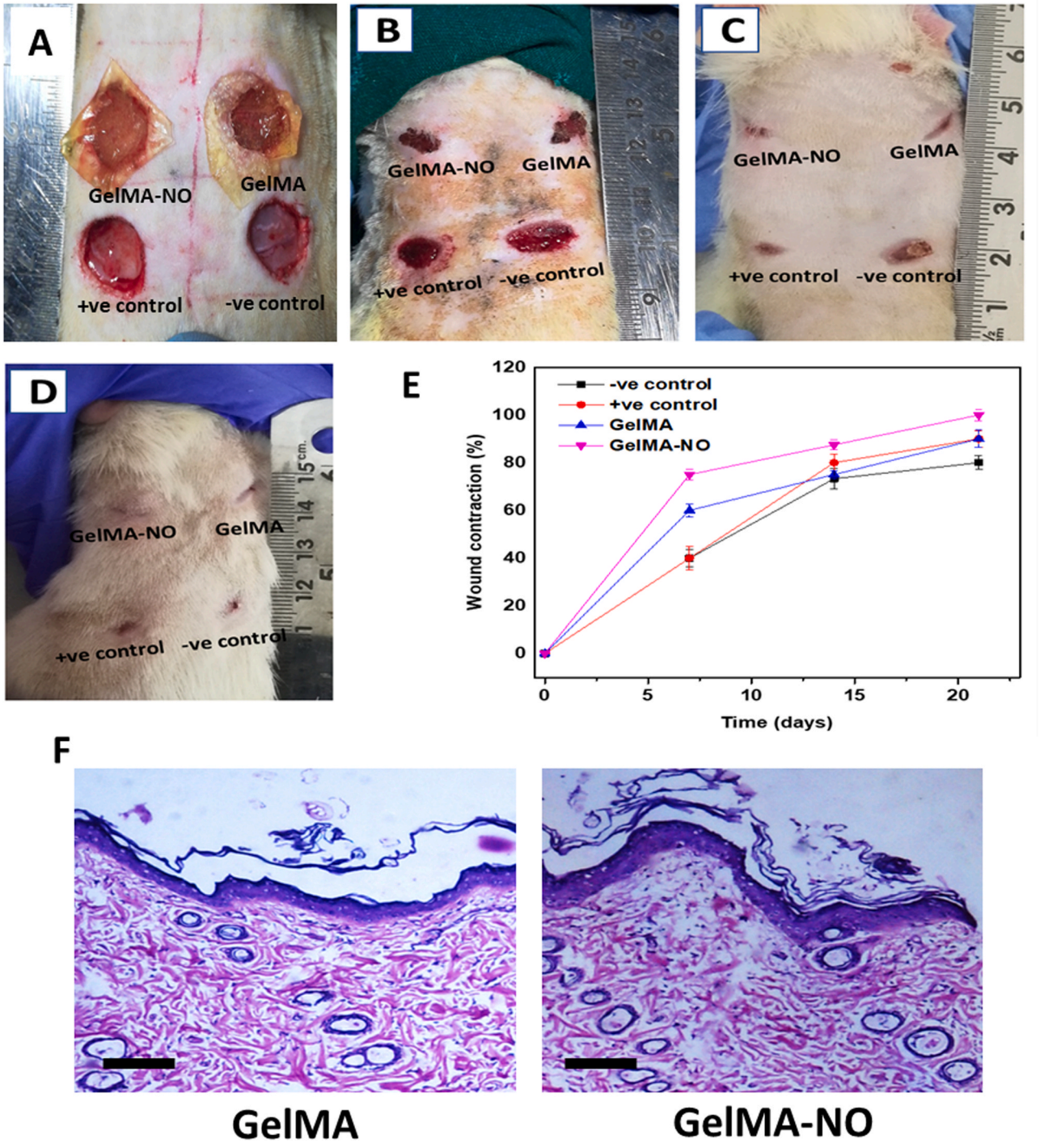

Fig. 5. Effect of NO donor loaded GelMA patches on diabetic wound healing. Photographs were taken on the first day (A), 7th day (B), 14th day (C) 21st day (D) of the study showing the wounds of diabetic rats treated with GelMA, GelMA-NO, betadine (+ve control), and untreated control (-ve control) wounds. Percentage of wound contraction in course of 21 days (E). The H & E stained histological images of skin tissue samples from the healed wounds which were treated with NO donor loaded GelMA and blank GelMA (F). Scale bar, 200 μm.

inflammation with scab formation, and the dermis seemed to be slightly necrotic (Fig. 5B). A considerable decrease in wound area was noted in all groups with a higher contraction in those treated with the GelMA-NO patch of concentration 1 G (GelMA-SNAP-0.08%). There was a slightest to medium exudation on the wounds treated with GelMA and GelMA-NO whereas both the controls were highly exudative.

The wound inflammation was reduced on day 14th, and observed new hair growth over the healed areas of wounds (Fig. 5**C**). The hair growth might be due to the rebuilding of the intact epidermis on the GelMA-NO, GelMA, and positive control groups. However, the untreated wounds showed relatively more minor hair growth. Among all the treatment groups, somewhat faster hair growth and rapid wound contraction were seen on the animals treated with GelMA-NO samples. Moreover, the remodeling of the epidermis showed promising wound healing efficacy of NO released from the GelMA-NO patch. On the final day of the study (21st day), the wound site treated with the GelMA-NO patch was fully healed and recovered with the normal dermal region and hair growth all around the wound area leaving only a light mark.

However, both positive and negative controls were not completely healed, leaving a large unhealed area without fur. The percentage of wound contraction was calculated to quantify the extent of wound healing, and the result is given in Fig. 5E. Both GelMA-NO and GelMA treated wounds showed higher wound contraction on the 7th day of the study itself. This trend of higher contraction was observed on the wounds treated with GelMA-NO throughout the study period. However, towards the end of the study, GelMA patches and positive control groups showed no significant difference in wound contraction. On the 21st day of study, 100% wound contraction was observed for the wounds treated with GelMA-NO patches. GelMA patches, positive controls, and untreated wounds showed 90.1 ± 2.9%, 90.3 ± 3.4%, and 80.1 ± 3.6% wound healing.

Obtained results suggest that NO enhance wound healing in diabetic rats. Endogenously, NO is produced through the enzyme nitric oxide synthase (NOS), through which three different NOS isoforms form [48]. Each encoded as an endothelial enzyme (eNOS), neuronal enzyme (nNOS), an inducible enzyme (iNOS). These isoforms are all expressed in skin tissue [49]. Such as nNOS can be found in keratinocytes, while eNOS has been observed in the basal epidermis layer of keratinocytes and dermal fibroblasts, and iNOS is detected in fibroblasts, keratinocytes, and endothelial cells [50]. Strong correlations suggest the reduced levels of NO leads to impaired wound healing in diabetic conditions [51–53]. Studies show that skin eNOS expression or NO levels have been considerably reduced in streptozotocin (STZ)- induced type 1 diabetic animals, resulting in a decreased healing process [51, 53, 54]. However, by performing skin gene therapy which restored eNOS expression and NO levels that accelerated the wound healing in (STZ)- induced type 1 diabetic animal [53]. With these diabetic conditions, NO donors were introduced to provide NO exogenously to the wound site to promote diabetic wound healing. Stallmeyer et al. demonstrated that a moderate level of NO enhances keratinocyte proliferation *in vitro* [55] and showed higher fibroblast proliferation [13,56]. Other studies suggest NO-releasing PVA based dressings improve the diabetic wound healing process [13, 57, 58].

Furthermore, NO inhibits infection by controlling the growth of bacteria during exogenous application and thus promotes the healing of wounds [26, 59–61]. The histopathological analysis indicates the higher re-epithelialization and complete formation of stratum corneum of the GelMA-NO wound in contrast to GelMA treated wounds (Fig. 5F). Moreover, a relatively thick epidermis can be observed for the GelMA-NO samples treated healed skin tissue than GelMA treated healed skin tissue. Also, it has been observed in Fig. 5F that thick hair follicles were present for GelMA-NO treated wounds in comparison to neat GelMA treated wounds. In our earlier study, a thin layer of the epidermis was noticed for the wound applied with GelMA samples [39]. Further, incorporating NO donor SNAP enhances cell proliferation and migration with accelerated angiogenic activity in a chick embryo model [13]. With the promising results obtained from this study, it can be recommended that NO-releasing GelMA patch possess high wound exudate uptake capacity, sustained NO-releasing behaviour, supports faster cell proliferation, and would be a promising formulation for rapid wound healing in chronic and diabetic wounds.

4. Conclusions

The improper treatment of chronic wounds and diabetic foot ulcers may lead to limb salvage or amputation, and the patient suffers from poor quality of life. To overcome this challenge, we have developed a biodegradable NO-releasing GelMA based wound healing patch. NO serves as the potent mediator for enhancing the reepithelization and remodelling process. The optimum concentrations of Ru and SPS based visible light crosslinking agents were used and showed a nontoxic and cell-friendly environment. The NO release study depicted prolonged and sustained release up to 80 h. Further, the NO releasing GelMA patch revealed greater cell viability, proliferation, and migration with the SNAP concentration of 0.08% (w/w). Moreover, the same concentration of NO releasing GelMA patch resulted in significant wound contraction and rapid wound healing compared to blank GelMA hydrogel and control groups on the diabetes-induced rat model. Given the above results, SNAP incorporated visible light crosslinked GelMA hydrogel can be suggested to develop clinically relevant wound healing patches that facilitate rapid wound healing when applied on diabetic wounds.

Conflict of interest statement

Authors declare that there's no financial/personal interest or belief that could affect the results, discussions or conclusions which are reported in this work.

Acknowledgements

This article was made possible by the NPRP12S-0310-190276 grant funded by the Qatar National Research Fund (a part of the Qatar Foundation). We also acknowledge the support provided by the Central Laboratories Unit (CLU) and Center for Advanced Materials (CAM), Qatar University, Qatar. Open Access funding provided by the Qatar National Library.

References

[1] K. Järbrink, G. Ni, H. Sönnergren, A. Schmidtchen, C. Pang, R. Bajpai, J. Car, The humanistic and economic burden of chronic wounds: a protocol for a systematic review, Syst. Rev. 6 (1) (2017) 15.
[2] P. Seedi, P. Salpea, S. Karuranga, I. Petersohn, B. Malanda, E.-W Gregg, N. Unvin, S.-H Wild, R. Williams, Mortality attributable to diabetes in 20-79 years old adults, 2019 estimates: results from the International Diabetes Federation Diabetes Atlas, 9th edition, Diabetes Res. Clin. Pract. (2020), 108086.
[3] R. Augustine, A. Hasan, N.K. Patan, A. Augustine, Y.-B Dalvi, R. Varghese, R. N. Unni, N. Kalarikkal, A.E. Al-Moustafa, S. Thomas, Titanium nanorods loaded PCL meshes with enhanced blood vessel formation and cell migration for wound dressing applications, Macromol. Biosci. 19 (7) (2019), 1900058.
[4] C.T. Hess, Checklist for factors affecting wound healing, Adv. Skin Wound Care 24 (4) (2011), 192.
[5] V. Falanga, Wound healing and its impairment in the diabetic foot, Lancet 366 (9498) (2005) 1736–1743.
[6] K. Järbrink, G. Ni, H. Sönnergren, A. Schmidtchen, C. Pang, R. Bajpai, J. Car, Prevalence and incidence of chronic wounds and related complications: a protocol for a systematic review, Syst. Rev. 5 (1) (2016) 152.
[7] P.J Kim, M. Heilala, J.S Steinberg, G.M. Weinraub, Bioengineered alternative tissues and hyperbaric oxygen in lower extremity wound healing, Clin. Podiatr. Med. Surg. 24 (3) (2007) 529–546.
[8] J.S. Steinberg, B. Werber, P.J. Kim, Bioengineered Alternative Tissues for the Surgical Management of Diabetic Foot Ulceration, in Surgical Reconstruction of the Diabetic Foot and Ankle, Lippincott, Williams & Wilkins Philadelphia, 2009, pp. 105–109.
[9] S.P. Zhong, Y.Z. Zhang, C.T. Lim, Tissue scaffolds for skin wound healing and dermal reconstruction, Wiley Interdiscip. Rev. Nanomed. Nanobiotechnol. 2 (5) (2010) 510–525.
[10] K. Kataria, A. Gupta, G. Rath, R.B. Mathur, S.R. Dhakate, In vivo wound healing performance of drug loaded electrospun composite nanofibers transdermal patch, Int. J. Pharm. 469 (1) (2014) 102–110.
[11] R. Ahmed, A. Afreen, M. Tariq, A.A. Zahid, M.S. Masoud, M. Ahmed, I. Ali, Z. Akram, A. Hasan, Bone marrow mesenchymal stem cells preconditioned with nitric oxide releasing chitosan/PVA hydrogel attenuate diabetic wound healing in rabbits, Biomed. Mater. 16 (3) (2020).
[12] Mhanna, R., A.J.T.E.f.A.O.R.M. Hasan, Smart Diagnostics, and P. Medicine, Introduction to tissue engineering. 2017. 1: p. 1–34.
[13] A.A. Zahid, R. Ahmed, S. Raza Ur Rehman, R. Augustine, M. Tariq, A. Hasan, Nitric oxide releasing chitosan-poly (vinyl alcohol) hydrogel promotes angiogenesis in chick embryo model, Int. J. Biol. Macromol. 136 (2019) 901–910.
[14] R. Augustine, A.A. Zahid, A. Hasan, M. Wang, T.J. Webster, CTGF loaded electrospun dual porous core-shell membrane for diabetic wound healing, Int. J. Nanomed. 14 (2019) 8573–8588.
[15] R. Augustine, S.R. Ur-Rehman, R. Ahmed, A.A. Zahid, M. Sharifi, M. Falahati, A. Hasan, Electrospun chitosan membranes containing bioactive and therapeutic agents for enhanced wound healing, Int. J. Biol. Macromol. (2020) 153–170.
[16] R. Augustine, et al., Crosslinking Strategies to Develop Hydrogels for Biomedical Applications, in Nano Hydrogels, Springer, 2021, pp. 21–57.
[17] M.A. Islam, T.E. Park, E. Reesor, K. Cherukula, A. Hasan, J. Firdous, B. Singh, S. K. Kang, Y.J. Choi, I.K. Park, C.S. Cho, Mucoadhesive chitosan derivatives as novel drug carriers, Curr. Pharm. Des. 21 (29) (2015) 4285–4309.

[18] R. Augustine, A. Zahid, A. Hasan, Y.B. Dalvi, Cerium oxide nanoparticle-loaded gelatin methacryloyl hydrogel wound-healing patch with free radical scavenging activity, ACS Biomater. Sci. Eng. 7 (1) (2020).

[19] R. Augustine, A. Hasan, Y.B Dalvi, S.R. Ur-Rehman, R. Varghese, R.N. Unni, H. C. Valcin, R. Alfkey, S. Thomas, A.E. Al-Moustafa, Growth factor loaded in situ photocrosslinkable poly(3-hydroxybutyrate-co-3-hydroxyvalerate)/gelatin methacryloyl hybrid patch for diabetic wound healing, Mater. Sci. Eng. C Mater. Biol. Appl. (2021), 111519.

[20] S.R. Ur-Rehman, R. Augustine, A.A. Zahid, R. Ahmed, M. Tariq, A. Hasan, Reduced graphene oxide incorporated gelma hydrogel promotes angiogenesis for wound healing applications, Int. J. Nanomed. 14 (2019), 9603.

[21] D. Devegowda, Human papillomavirus screening: time to add molecular methods with cytology, Int. J. Health Allied Sci. 3 (3) (2014) 145.

[22] F.R. de-Gruijl, H.J. van-Kranen, L.H. Mullenders, UV-induced DNA damage, repair, mutations and oncogenic pathways in skin cancer, J. Photochem. Photobiol. B 63 (1–3) (2001) 19–27.

[23] J. Dahle, E. Kvam, T. Stokke, Bystander effects in UV-induced genomic instability: antioxidants inhibit delayed mutagenesis induced by ultraviolet A and B radiation, J. Carcinog. 4 (2005) 11.

[24] D. Kulms, E. Zeise, B. Pöppelmann, T. Schwarz, DNA damage, death receptor activation and reactive oxygen species contribute to ultraviolet radiation-induced apoptosis in an essential and independent way, Oncogene 21 (38) (2002) 5844–5851.

[25] K.S Lim, B.S Schon, N.V Mekhileri, G.C.J. Brown, C.M Chia, S. Prabhakar, G. J Hooper, T.B.F. Woodfield, New visible-light photoinitiating system for improved print fidelity in gelatin-based bioinks, ACS Biomater. Sci. Eng. 2 (10) (2016).

[26] M. VanWagner, J. Rhadigan, M. Lancina, A. Lebovsky, G. Romanowicz, H. Holmes, M.A. Brunette, K.L. Snyder, M. Bostwick, B.P. Lee, M.C. Frost, R.M. Rajachar, S-nitroso-N-acetylpenicillamine (SNAP) derivatization of peptide primary amines to create inducible nitric oxide donor biomaterials, ACS Appl. Mater. Interfaces 5 (17) (2013) 8430–8439.

[27] J.S. Isenberg, L.A. Ridnour, M.G. Espey, D.A. Wink, D.D. Roberts, Nitric oxide in wound-healing, Microsurg. Off. J. Int. Microsurg. Soc. Eur. Fed. Soc. Microsurg. 25 (5) (2005) 442–451.

[28] Q. Xing, et al., Effects of local nitric oxide release on human mesenchymal stem cell attachment and proliferation on gelatin hydrogel surface. 2013. 1(4): p. 224–232.

[29] W. Schuurman, P.A. Levett, M.W. Pot, P.R. van Weeren, W.J. Dhert, D. W. Hutmacher, F.P. Melchels, T.J. Klein, J. Malda, Gelatin-methacrylamide hydrogels as potential biomaterials for fabrication of tissue-engineered cartilage constructs, Macromol. Biosci. 13 (5) (2013) 551–561.

[30] J.W. Nichol, S.T. Koshy, H. Bae, C.M. Hwang, S. Yamanlar, A. Khademhosseini, Cell-laden microengineered gelatin methacrylate hydrogels, Biomaterials 31 (21) (2010) 5536–5544.

[31] A. Hasan, A. Paul, A. Memic, A. Khademhosseini, A multilayered microfluidic blood vessel-like structure, Biomed. Microdevices 17 (5) (2015) 1–13.

[32] A. Paul, V. Manoharan, D. Krafft, A. Assmann, J.A. Uquillas, S.R. Shin, A. Hasan, M. A. Hussain, A. Memic, A.K. Gaharwar, A. Khademhosseini, Nanoengineered biomimetic hydrogels for guiding human stem cell osteogenesis in three dimensional microenvironments, J. Mater. Chem. B 4 (20) (2016) 3544–3554.

[33] R. Ahmed, M. Tariq, I. Ali, R. Asghar, P. Noorunnisa Khanam, R. Augustine, A. Hasan, Novel electrospun chitosan/polyvinyl alcohol/zinc oxide nanofibrous mats with antibacterial and antioxidant properties for diabetic wound healing, Int. J. Biol. Macromol. 120 (2018) 385–393.

[34] R. Augustine, A. Augustine, N. Kalarikkal, S. Thomas, Fabrication and characterization of biosilver nanoparticles loaded calcium pectinate nano-micro dual-porous antibacterial wound dressings, Prog. Biomater. 5 (3–4) (2016) 223–235.

[35] B.L. Furman, Streptozotocin-induced diabetic models in mice and rats, Curr. Protoc. Pharmacol. 70 (1) (2015).

[36] N.M. James, et al., Effect of Metformin on Alveolar Bone Loss in Type 2 Diabetic Rat Model with Experimental Periodontitis.

[37] R. Augustine, A. Hasan, N.K. Patan, Y.B Dalvi, R. Varghese, A. Antony, R.N. Unni, N. Sandhyarani, A.E. Al-Moustafa, Cerium oxide nanoparticle incorporated electrospun poly(3-hydroxybutyrate- co-3-hydroxyvalerate) membranes for diabetic wound healing applications, ACS Biomater. Sci. Eng. (2019).

[38] Y. Zu, Y. Zhang, X. Zhao, C. Shan, S. Zu, K. Wang, Y. Li, Y. Ge, Preparation and characterization of chitosan–polyvinyl alcohol blend hydrogels for the controlled release of nano-insulin, Int. J. Biol. Macromol. 50 (1) (2012) 82–87.

[39] R. Augustine, A. Hasan, Y.B. Dalvi, S.R. Ur-Rehman, R. Varghese, R.N. Unni, H. C. Yalcin, R. Alfkey, S. Thomas, A.E. Al-Moustafa, Growth factor loaded in situ photocrosslinkable poly(3-hydroxybutyrate-co-3-hydroxyvalerate)/gelatin methacryloyl hybrid patch for diabetic wound healing, Mater. Sci. Eng. C Mater. Biol. Appl. (2020) 111519.

[40] G.E. Gierke, M. Nielsen, M.C. Frost, S-Nitroso-N-acetyl-D-penicillamine covalently linked to polydimethylsiloxane (SNAP–PDMS) for use as a controlled photoinitiated nitric oxide release polymer, Sci.Technol. Adv. Mater. 12 (5) (2011) 055007.

[41] C. Vogt, Q. Xing, W. He, B. Li, M.C. Frost, F. Zhao, Fabrication and characterization of a nitric oxide-releasing nanofibrous gelatin matrix 14 (8) (2013) 2521–2530.

[42] Y. Wo, E.J. Brisbois, A. Colletta, J. Wu, T.C. Major, C. Xi, R.H. Barlett, A.J. Matzger, M.E. Meyerhoff, Origin of long-term storage stability and nitric oxide release behavior of carbosil polymer doped with S-nitroso-N-acetyl-D-penicillamine, ACS Appl. Mater. Interfaces 7 (40) (2015) 22218–22227.

[43] N.A. Peppas, J.Z. Hilt, A. Khademhosseini, R. Langer, Hydrogels in biology and medicine: from molecular principles to bionanotechnology, Adv. Mater. 18 (11) (2006) 1345–1360.

[44] A. Soneja, M. Drews, T. Malinski, Role of nitric oxide, nitroxidative and oxidative stress in wound healing, Pharmacol. Rep. 57 (2005).

[45] W.R.J.A.E.M. Reenstra, Decreased proliferation and cellular signaling in primary dermal fibroblasts derived from diabetics versus non-diabetic sibling controls. 2001. 8: p. 519.

[46] S. Frank, B. Stallmeyer, H. Kämpfer, N. Kolb, J. Pfeilschifter, Nitric oxide triggers enhanced induction of vascular endothelial growth factor expression in cultured keratinocytes (HaCaT) and during cutaneous wound repair, FASEB J. 13 (14) (1999) 2002–2014.

[47] Y.C. Hsu, M. Hsiao, L.F. Wang, Y.W. Chien, W.R. Lee, Nitric oxide produced by iNOS is associated with collagen synthesis in keloid scar formation, Nitric Oxide 14 (4) (2006) 327–334.

[48] O.W. Griffith, D.J. Stuehr, Nitric oxide synthases: properties and catalytic mechanism, Annu. Rev. Physiol. 57 (1) (1995) 707–734.

[49] S. Frank, H. Kämpfer, C. Wetzler, J. Pfeilschifter, Nitric oxide drives skin repair: novel functions of an established mediator, Kidney Int. 61 (3) (2002) 882–888.

[50] J. dong-Luo, A.F. Chen, Nitric oxide: a newly discovered function on wound healing, Acta Pharmacol. Sin. 26 (3) (2005) 259–264.

[51] M.R. Schaffer, U. Tantry, S.S. Gross, H.L. Wasserburg, A. Barbul, Nitric oxide regulates wound healing, J. Surg. Res. 63 (1) (1996) 237–240.

[52] M.R. Schäffer, U. Tantry, P.A. Efron, G.M. Ahrendt, F.J. Thornton, A. Barbul, Diabetes-impaired healing and reduced wound nitric oxide synthesis: a possible pathophysiologic correlation, Surgery 121 (5) (1997) 513–519.

[53] J.D. Luo, Y.Y. Wang, W.L. Fu, J. Wu, A.F. Chen, Gene therapy of endothelial nitric oxide synthase and manganese superoxide dismutase restores delayed wound healing in type 1 diabetic mice, Circulation 110 (16) (2004) 2484–2493.

[54] B. Stallmeyer, M. Anhold, C. Wetzler, K. Kahlina, J. Pfeilschifter, S. Frank, Regulation of eNOS in normal and diabetes-impaired skin repair: implications for tissue regeneration, Nitric Oxide 6 (2) (2008) 168–177.

[55] B. Stallmeyer, H. Kämpfer, N. Kolb, J. Pfeilschifter, S. Frank, The function of nitric oxide in wound repair: inhibition of inducible nitric oxide-synthase severely impairs wound reepithelialization, J. Invest. Dermatol. 113 (6) (1999) 1090–1098.

[56] A. Schwentker, T.R. Billar, Inducible nitric oxide synthase: from cloning to therapeutic applications, World J. Surg. 26 (7) (2002) 772–778.

[57] M.B. Witte, T. Kiyamma, A. Barbul, Nitric oxide enhances experimental wound healing in diabetes, Br.J. Surg. 89 (12) (2002) 1594–1601.

[58] K.S.B. Masters, S.J. Leibovich, P. Belem, J.L. West, L.A.P. Warren, Effects of nitric oxide releasing poly(vinyl alcohol) hydrogel dressings on dermal wound healing in diabetic mice, Wound Repair Regen. 10 (5) (2002) 286–294.

[59] S. Kumar, R.K. Singh, T. Bhardwaj, Therapeutic role of nitric oxide as emerging molecule, Biomed. Pharmacother. 85 (2017) 182–201.

[60] Y. Li, P.I. Lee, Controlled nitric oxide delivery platform based on S-nitrosothiol conjugated interpolymer complexes for diabetic wound healing, Mol. Pharm. 7 (1) (2010) 254–266.

[61] D.O. Schairer, J.S. Chouake, J.D. Nosanchuk, A.J. Friedman, The potential of nitric oxide releasing therapies as antimicrobial agents, Virulence 3 (3) (2012) 271–279.